ARCHIVE OF MECHANICAL ENGINEERING

DOI: 10.24425/ame.2023.146849 2023, Vol. 70, No. 3, pp. 433–452

Karim BOUAOUICHE [1], Yamina MENASRIA [1], Dalila KHALFA [1]

Detection and diagnosis of bearing defects using vibration signal processing

Received 15 February 2023, **Revised** 18 August 2023, **Accepted** 22 August 2023, **Published online** 30 September 2023

Keywords: vibration signal, bearing, signal processing, envelope spectrum, fault frequency

This work presents an analysis of vibration signals for bearing defects using a proposed approach that includes several methods of signal processing. The goal of the approach is to efficiently divide the signal into two distinct components: a meticulously organized segment that contains relatively straightforward information, and an inherently disorganized segment that contains a wealth of intricately complex data. The separation of the two component is achieved by utilizing the weighted entropy index (WEI) and the SVMD algorithm. Information about the defects was extracted from the envelope spectrum of the ordered and disordered parts of the vibration signal. Upon applying the proposed approach to the bearing fault signals available in the Paderborn university database, a high amplitude peak can be observed in the outer ring fault frequency (45.9 Hz). Likewise, for the signals available in XJTU-SY, a peak is observed at the fault frequency (108.6 Hz).

1. Introduction

Rotating machines rely on bearings to support dynamic loads and transmit movements between components, making the bearing a critical component [1]. The structure of the bearing generally includes an outer ring, an inner ring, a cage, and a rolling element [1]. Incorrect assembly or overload can lead to defects in bearings, manifested as wear, fatigue, corrosion, deformation, and a combination of these defects causing undesirable vibrations and a reduction in the lifespan [2]. Defect detection is carried out through various failure detection techniques such as acoustic emission measurements, thermography, and vibration analysis [3]. Among

✉ Karim BOUAOUICHE, email: karimbouaouiche@gmail.com

[1]Electromechanical Engineering Laboratory, Badji Mokhtar University, Annaba, Algeria.

ORCIDs: K.B.: 0000-0003-0740-3681; Y.M.: 0000-0003-0807-7822; D.K.: 0000-0002-9298-7660

all the detection techniques, vibration analysis is widely used as a monitoring and control technique for rotating equipment [4].

The vibration signal is measured by a measurement chain comprising sensors and a data system [4]. The choice of sensors depends on the frequency range, with displacement sensors used in the low-frequency range, velocity sensors in the mid-frequency range, and the accelerometers in the high-frequency range [4]. Vibration signal analysis methods for defect detection are classified into two categories: one is based on the design and analysis of a model associated with the system or the rotating machine, such as Markov chains and artificial neural networks [5]. The second category of methods focuses on feature extraction from vibration signals, whether in the time domain, frequency domain, or time-frequency domain [5]. Signal analysis in the time domain is based on the calculation and comparison of values of statistical indicators to distinguish between healthy and faulty states of the bearing [6]. Several statistical parameters are used, such as root mean square (RMS), kurtosis, and standard deviation [6]. Signal processing in the frequency domain involves spectral analysis, which includes the Fourier transformation to convert the signal from the time domain to the frequency domain [7]. The wavelet transform, the Wigner-Ville distribution, and the Hilbert-Huang transform are the tools used in the time-frequency domain [8].

Methods for detecting bearing faults from vibration signals have been developed with the aim of improving diagnostic accuracy. This has led to the use of algorithms for decomposing complex signals into several simple components, such as variational mode decomposition (VMD) [9] and successive variational mode decomposition (SVMD) [10]. Thus, the vibration signal can be considered as a convolution product between the fault impulse and the transfer function of the path between the fault source and the sensor [11]. In this context, signal deconvolution methods are used in diagnostics, such as minimum entropy deconvolution [12]. Moreover, the Kurtogram [13] and the Autogram [14] are important methods for the efficient selection of frequency bands in the vibration signal, containing information about faults. Additionally, deep learning techniques are applied in the bearing fault diagnosis, such as Convolutional Neural Networks (CNN) and Deep Belief Networks (DBN) [15].

In article [5], we present an approach for detecting anomalies within rotating machines. This approach is based on reconstructing a signal containing impulses by leveraging both kurtosis and the Feature Mode Decomposition (FMD) method. Regarding the FMD method, we propose an innovative criterion for identifying input parameters. Once the parameters of the FMD method are determined, the signal is decomposed into multiple components. The components with kurtosis values greater than three are summed to create a new signal, from which defect-related information is extracted by applying the Kurtogram. Furthermore, the presence of a high-amplitude peak in the spectrum allows for the detection of the defect.

Furthermore, within article [16], we examine an approach for anomaly detection. This strategy is based on the principle of comparing information from the

normal state and the faulty state of the bearing. In this approach, a criterion based on the maximum correlation value, as well as a kurtosis value greater than three, is proposed for selecting a single component obtained after signal decomposition. The fault detection approach is divided into two parts: the first one indicates the presence of a fault, and once the presence is indicated, the second part engages in locating the fault. The localization is accomplished by comparing the frequencies of the peaks obtained through envelope analysis with the spectra of a single component selected after signal decomposition.

In this study, we analyze the complexity of the signals. Typically, signal complexity is expressed as a single, simple number, but in this paper, we introduce an indicator called the WKI that allows distinguishing between two signal components that vary over time: one ordered and the other disordered. Moreover, we highlight an algorithm aimed at optimizing the input parameters of the SVMD method. The combination of peaks in the envelope spectra of the ordered and disordered components enables the detection and localization of defects. Moreover, it is discovered that the original vibration signal is complex, making data interpretation impossible. However, after evaluating the complexity of the data, it becomes possible to interpret the data in a simpler manner.

2. Methods

The MATLAB code of the proposed approach incorporates a series of organized methods, as illustrated in Fig. 1, for analyzing vibratory signals.

2.1. Noise removal of the signal

To eliminate noise in vibration signals, it is necessary to use the Donoho algorithm, which involves the following steps [17]:

- Discretization of the continuous signal.
- Decomposition of the signal will be achieved via the discrete wavelet transform (DWT), and the resultant DWT coefficients will be calculated using the following formula [18]:

$$W_{j,k} = 2^{-j/2} \int_{-\infty}^{+\infty} x(t)\overline{\psi(2^{-j}t - k)}\,\mathrm{d}t\,, \tag{1}$$

  $\overline{\psi}$ is conjugate complex of ψ.
- Applying the threshold (λ) to the wavelet coefficients:

$$\lambda = \sqrt{2\sigma \log(n)}, \tag{2}$$

  where: n is length of signal, σ is variance of noise.

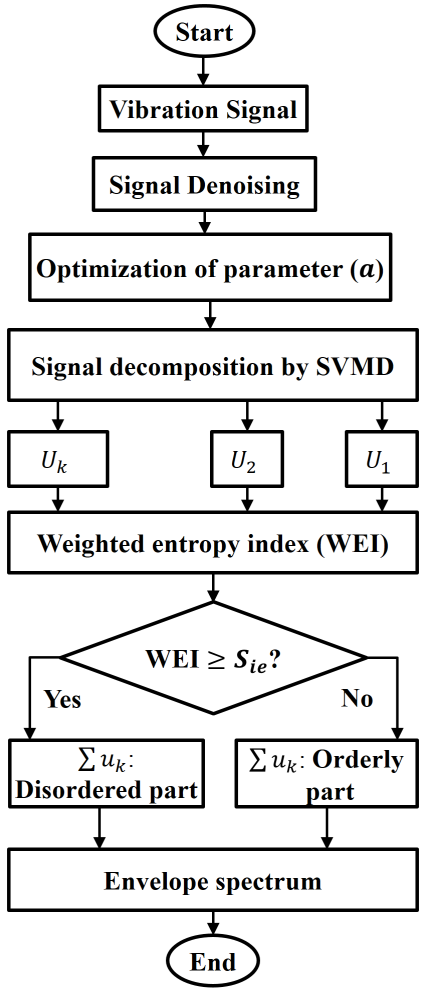

Fig. 1. Proposed approach

- Performing the inverse discrete wavelet transform (IDWT) is necessary to obtain the signal without noise, and the subsequent formula must use to compute the IDWT [18]:

$$x(t) = \sum_{i=-\infty}^{+\infty} \sum_{k=-\infty}^{+\infty} W_{j,k} \psi_{j,k}(t). \tag{3}$$

The mother wavelet $\psi(t)$ undergoes scaling or shifting to produce $\psi_{j,k}(t)$.

Donoho de-noising algorithm requires two input parameters, namely the mother wavelet type and the decomposition level. For our study, the chosen mother wavelet is Daubechies of order three (db3), and the decomposition level selected is $L = 2$.

2.2. SVMD method

The successive application of the variational mode extraction (VME) algorithm constitutes the implementation of the successive variational mode decomposition (SVMD) method [10]. SVMD method decomposes a signal $f(t)$ into several modes (u) with an unprocessed part $fu(t)$ [10]:

$$f(t) = fu(t) + \sum_{i=1}^{L} u_i(t). \tag{4}$$

The SVMD algorithm is defined by the equations and steps presented below [10]:

Input $f(t)$, Set $a,\ e1,\ e2$

Initialize $L \longleftarrow 0$

Repeat

$L \longleftarrow L + 1$

Initialize $\hat{u}_L^1,\ \hat{\lambda}^1,\ \omega_L^1,\ n \longleftarrow 0$

Repeat

$n \longleftarrow n + 1$

1. Update $\hat{u}_L$ for all $\omega \geq 0$:

$$\hat{u}_L^{n+1}(\omega) = \frac{\hat{f}(\omega) + a^2\left(\omega - \omega_L^n\right)^4 \hat{u}_L^n(\omega) + \frac{\hat{\lambda}(\omega)}{2}}{\left[1 + a^2(\omega - \omega_L^n)^4\right]\left[1 + 2a(\omega - \omega_L^n)^2 + \sum_{i=1}^{L-1} \frac{1}{a^2(\omega - \omega_i)^4}\right]}$$

2. Update ω_L:

$$\omega_L^{n+1} = \frac{\int_0^\infty \omega|\hat{u}_L^{n+1}(\omega)|^2 d\omega}{\int_0^\infty |\hat{u}_L^{n+1}(\omega)|^2 d\omega}$$

3. Dual ascent for all $\omega \geq 0$:

$$\hat{\lambda}^{n+1} = \hat{\lambda}^n + \tau\left[\hat{f}(\omega) - \hat{u}_L^{n+1} + \frac{a^2(\omega - \omega_L^{n+1})^4\left(\hat{f}(\omega) - \hat{u}_L^{n+1}(\omega) - \sum_{i=1}^{L-1}\hat{u}_i(\omega) + \frac{\hat{\lambda}(\omega)}{2}\right) - \sum_{i=1}^{L-1}\hat{u}_i(\omega)}{1 + a^2(\omega - \omega_L^{n+1})^4} + \sum_{i=1}^{L-1} u_i^{n+1}(\omega)\right]$$

Until convergence: $\dfrac{\left\|\hat{u}_L^{n+1} - \hat{u}_L^n\right\|_2^2}{\|\ \hat{u}_L^n\ \|_2^2} < e1$

Until convergence: $\left|\sigma^2 - \dfrac{1}{T}\left\|f(t) - \sum_{i=1}^{L} u_L(t)\right\|_2^2\right| \Big/ \sigma^2 < e2$

The SVMD algorithm takes (a) and $(e1,\ e2)$ as input parameters. The parameter (a) is typically set to a large value for balancing constraints [10].

The stop convergence value $(e1,\ e2)$ is typically set to 10^{-6} [10]. The SVMD algorithm addresses the issue of optimizing the number of modes and continues the

search for new modes until the power of the remaining signal becomes nearly equal to that of the white noise (σ^2) [10]. The stopping criterion of the SVMD algorithm is the sensitivity of the power of the final mode with respect to the frequency (ω) [10]. (λ): denotes the Lagrange multiplier [10].

2.2.1. Optimization of parameters

An algorithm based on feedback and cross-correlation value (C) between the original signal and the sum of modes obtained after decomposition must be used to optimize the constraint balancing parameter (a). Fig. 2 depicts the flowchart of the algorithm.

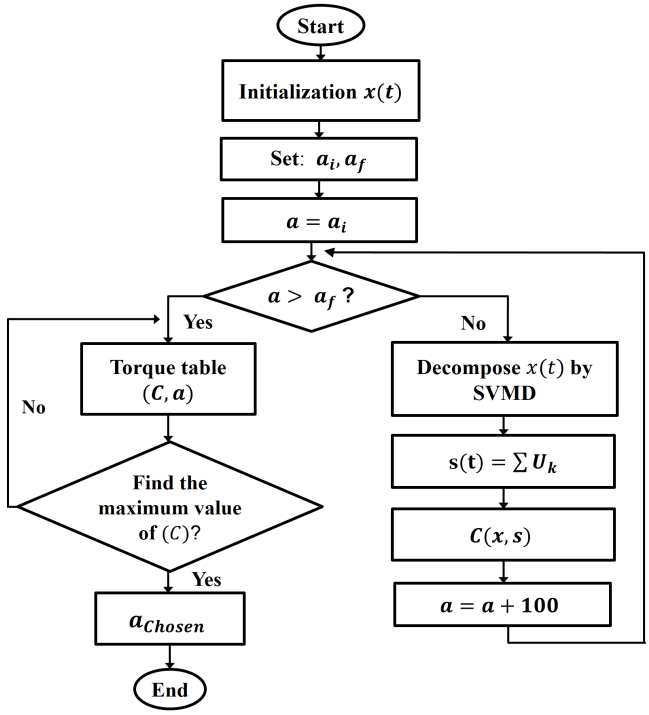

Fig. 2. Flowchart of the algorithm

The formula below defines the cross correlation function [19], which must be utilized to measure the similarity between two signals [20]:

$$C_{x,y}(\tau) = E[x(t)s(t+\tau)], \tag{5}$$

where: $E[.]$ – esperance, τ – time shift parameter.

Initial and final values (a_i, a_f) are randomly assigned to the parameter (a) in order to introduce variation. The desired value of a_{chosen} is determined by the highest values of cross correlation between the noise-free original signal and the sum of (u_k) obtained during the implementation of the SVMD algorithm on $a \in [a_i, a_f]$.

2.3. Weighted entropy index (WEI)

A novel metric called the weighted entropy index *WEI* is proposed, which aims to partition the signal into two segments, one being orderly and the other being disorderly. The construction of WEI involves combining kurtosis (Ku) with Shannon entropy (H) and the Hjorth complexity parameter (Cm):

$$WEI = Cm \times |H| \times Ku. \tag{6}$$

The selection of the three preceding parameters for building *WEI* must base on the intricacy of the signal, as indicated in the definition of each parameter:

- Information entropy is a concept of thermodynamic origin and is used to measure the complexity of the system, if the entropy value is lower, the system considered more organized, while in the contrary scenario, it suggests a greater degree of disorder. The Shannon formula is used for the computation of information entropy [21]:

$$H(x) = -\sum_{i=1}^{n} P(x_i) \log P(x_i), \tag{7}$$

  where $P(x_i)$ represents the probability of x_i in the system.
- The Hjorth parameter is a statistical characteristic of a signal in the time domain and comprises three types: activity, mobility, and complexity [22]. This paper focuses on the Hjorth complexity parameter, which is computed using the following formula [22]:

$$Cm = \frac{\sigma_{dd}\sigma_x}{\sigma_d^2}, \tag{8}$$

  where: σ_x is standard deviation of the signal (x), σ_d is standard deviation of the first derivative of (x), σ_{dd} is standard deviation of the second derivative of (x).
  The Hjorth complexity parameter quantifies the resemblance between a signal and a pure sine wave, as the parameter value approaches one, the signal form becomes increasingly similar to that of a sine wave [23].
- Kurtosis is employed in diagnosis and is particularly responsive to impulse signals, such as in the case of bearings [24]. A healthy bearing has a kurtosis value lower than three, while a faulty one exhibits a substantial increase in kurtosis value [24]. The following equation defines kurtosis [25]:

$$Ku = \frac{\frac{1}{N}\sum_{i=1}^{N}(x_i - \overline{x})^4}{\left(\frac{1}{N}\sum_{i=1}^{N}(x_i - \overline{x})^2\right)^2}, \tag{9}$$

  where: N – sample size, x_i – samples, $\overline{x}$ – mean.

As per the concept of the weighted entropy index (*WEI*), the signal $x(t)$ can be divided into two parts, separated by a threshold.

After decomposing the vibration signal using SVMD, the proposed threshold (S_{ie}) is equivalent to the *WEI* mean.

$$S_{ie} = \frac{\sum_{k=1}^{K} WEI_k}{K}, \tag{10}$$

where: K – total number of modes, WEI_k – weighted entropy index of each mode.

The ordered part (OP) corresponds to the total of modes (u_k), which display *WEI* values below S_{ie}, while the disordered part (DP) is the sum of (u_k), which denotes the values of *WEI* greater than S_{ie}.

$$\begin{aligned} OP(t) &= \sum_{k=1}^{K} u_k(t) \quad \text{with } WKI \text{ for each } (u); \quad WEI_k \leq S_{ei}, \\ DP(t) &= \sum_{k=1}^{K} u_k(t) \quad \text{with } WKI \text{ for each } (u); \quad WEI_k > S_{ei}, \end{aligned} \tag{11}$$

$$x(t) = OP(t) + DP(t). \tag{12}$$

In addition, both parts are defined as follows:

- The disordered part comprises a pulse train with intricate information and is dissimilar to sine waves.
- The ordered part contains a few pulses with relatively complex information, which are similar to sine waves.

2.4. Envelope spectrum

The envelope spectrum is the final diagnostic step used to extract fault frequencies from bearing components, it is determined through the Hilbert and Fourier transformations [26].

The following equation represents the Hilbert transform for a vibration signal $x(t)$ [27]:

$$H[x(t)] = x(t) * \frac{1}{\pi t}, \tag{13}$$

where: $*$ denotes convolution product.

The analytical signal is obtained through the following calculation [27]:

$$z(t) = x(t) + jH[x(t)] \Leftrightarrow z(t) = E(t)e^{j\psi(t)}. \tag{14}$$

The envelope of the vibration signal $x(t)$ can be calculated by taking the absolute value of the analytical signal, as shown in the following equation [27]:

$$E(t) = |z(t)|. \tag{15}$$

The envelope spectrum enables the identification of high amplitude peaks at the theoretical frequencies corresponding to bearing component defects [28].

A peak is the maximum amplitude value of a signal, which can be computed using the following formula [29]:

$$Peak = \max |x(t)|. \tag{16}$$

The defect frequencies of the bearing components are determined from the geometrical parameters, as shown in Table 1 [30].

Table 1. Defect frequencies

Components	Formulas
Outer race	$F_{or} = \frac{z \times Fr}{2}\left(1 - \frac{d}{Dm}\cos(a)\right)$
Inner race	$F_{ir} = \frac{z \times Fr}{2}\left(1 + \frac{d}{Dm}\cos(a)\right)$
Cage	$F_c = \frac{Fr}{2}\left(1 - \frac{d}{Dm}\cos(a)\right)$
Rolling element	$F_{re} = \frac{Fr \times Dm}{2d}\left(1 - \frac{d^2}{Dm^2}\cos^2(a)\right)$

where symbols denote:
z – number of rolling elements, Dm – pitch diameter, a – angle of contact, d – rolling element diameter, Fr – operating speed.

3. Experimental study

The proposed approach performance was evaluated by analyzing two vibration signals of bearing defects from two different databases, namely XJTU-SY and Paderborn University.

3.1. XJTU-SY bearing database

In the XJTU-SY database, a test strip has been created to measure the vibration signals of an LDK UER204 type bearing. The test strip contains a set of elements, as shown in Fig. 3 [31].

The measurement of the vibration amplitude of the bearing is performed using two accelerometers of the PCB 352C33 type, one mounted on the horizontal axis and the other on the vertical axis. The signals were sampled at a frequency of 25.6 kHz [31].

By utilizing the geometric parameters of the bearing found in reference [31] and the formulas presented in Table 1, it is possible to determine the defect frequencies for the various components of the bearing, as expressed by Table 2.

The provided vibration signal underwent processing using the approach outlined in Table 3.

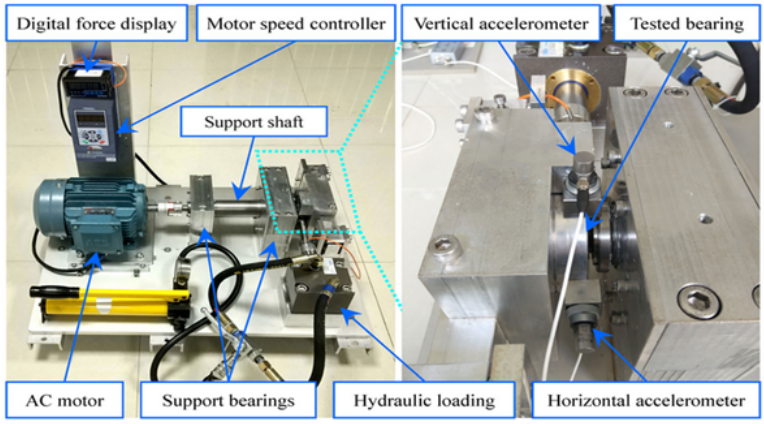

Fig. 3. Test strip used in the XJTU-SY database

Table 2. The values of frequencies

Parameters	Defect frequency
Outer race diameter 39.8 mm	$F_{or} = 3.0830Fr$
Inner race diameter 29.3 mm	$F_{ir} = 4.9169Fr$
Ball diameter 7.92 mm	$F_c = 0.3853Fr$
Pitch diameter 34.55 mm	$F_{re} = 2.066Fr$
Number of balls 8	
Angle of contact 0°	

Table 3. Vibration signal

Operating condition	Failed component	Fault frequency
Operating speed 35 Hz/Load 12 kN	Outer race	107.9 Hz

3.1.1. Results and discussion

- After the signal is de-noised, its spectrum becomes complex due to the presence of multiple peaks at different frequencies, as illustrated in Figs. 4 and 5.
- By conducting an optimization algorithm on the interval [100; 500], the optimal value of parameter (a) was determined as $a_{chosen} = 200$, which is depicted in Table 4.
- Signal decomposition using the SVMD algorithm produced six modes for the horizontal vibration signal and four modes for the vertical vibration signal, as shown in Figs. 6 and 7.
- Table 5 presents the values for each mode in the weighted entropy index (*WEI*). Based on these values and thresholds, the ordered and disordered segments of the horizontal and vertical vibration signals are defined as follows:

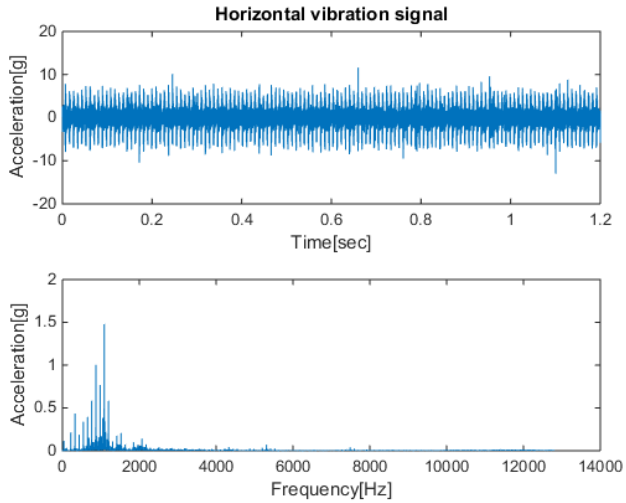

Fig. 4. Horizontal vibration signal

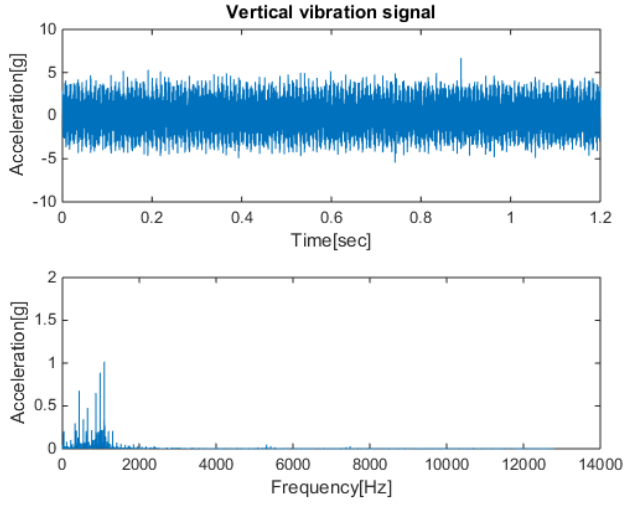

Fig. 5. Vertical vibration signal

Table 4. Correlation values

a	Horizontal signal correlation $\times 10^5$	Vertical signal correlation $\times 10^5$
100	2.7918	1.4220
200	2.7944	1.4221
300	2.7920	1.4200
400	2.7762	1.4196
500	2.7544	1.4140

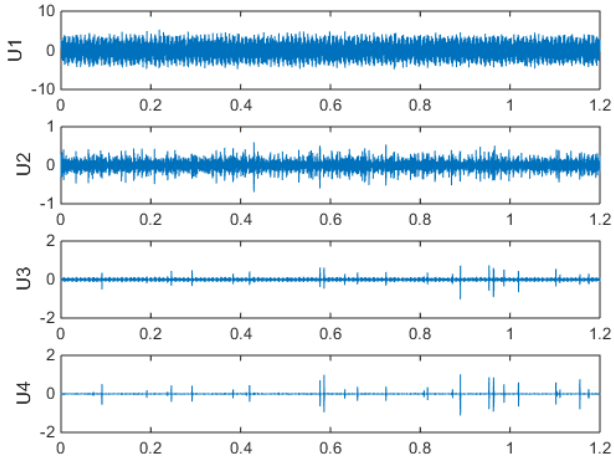

Fig. 6. Vertical signal modes

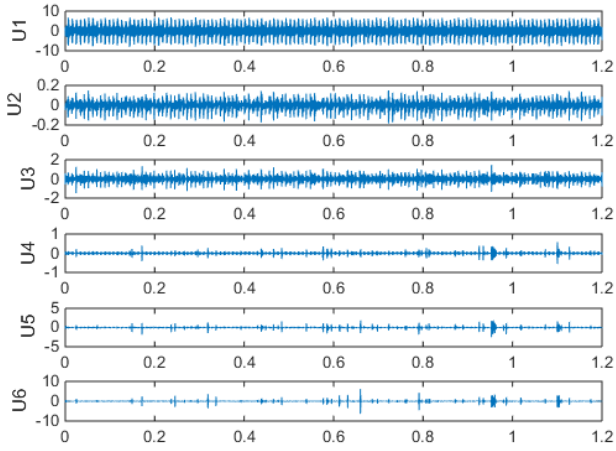

Fig. 7. Horizontal signal modes

– The thresholds for the horizontal and vertical vibration signals have been established.

$$SH_{ie} = 6.7044 \times 10^5, \quad SV_{ie} = 2.85325 \times 10^5. \tag{17}$$

– The ordered and disordered parts of the horizontal and vertical vibration signals:

$$DP_V(t) = DP_H(t) = u_1(t), \tag{18}$$

$$OP_H(t) = \sum_{k=2}^{6} u_k(t), \quad OP_V(t) = \sum_{k=2}^{4} u_k(t), \tag{19}$$

Table 5. The values of WEI

Modes	WEI of horizontal signal$\times 10^6$	WEI of vertical signal$\times 10^6$
u_1	3.3220	1.0454
u_2	0.0020	0.0128
u_3	0.0318	0.0250
u_4	0.0076	0.0581
u_5	0.0702	
u_6	0.5891	

- The envelope spectrum (Figs. 8 and 9) of the ordered and disordered segments of the horizontal and vertical vibration signals display a significant peak with high amplitude at a frequency of 108.6 Hz, this frequency value is in close proximity to the fault frequency of the outer ring, which is 107.9 Hz.

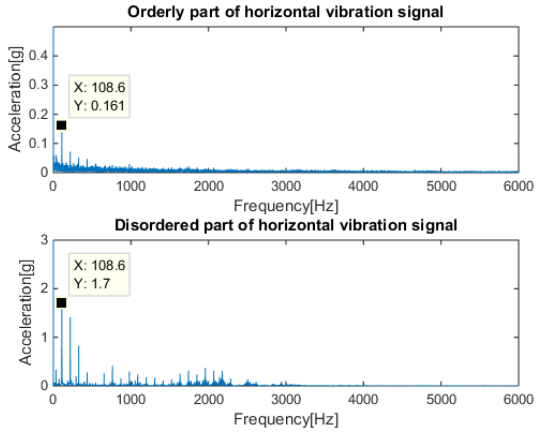

Fig. 8. Envelope spectrum of horizontal signal

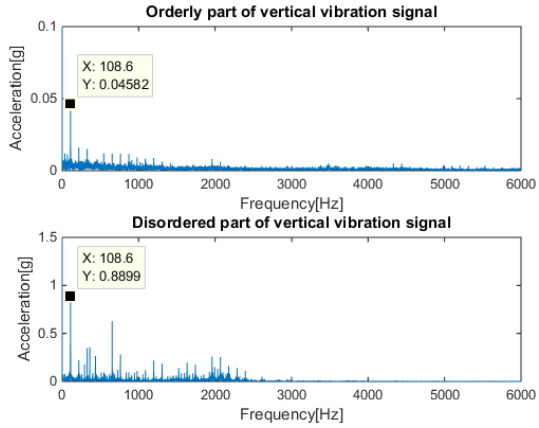

Fig. 9. Envelope spectrum of vertical signal

3.2. Paderborn University database

In the Paderborn University database, we find the vibration signals of the 6203-FAG type ball bearing, obtained from a test bench comprising an electric motor, a shaft, a bearing test module, a flywheel, and a load motor, as shown in Fig. 10 [32].

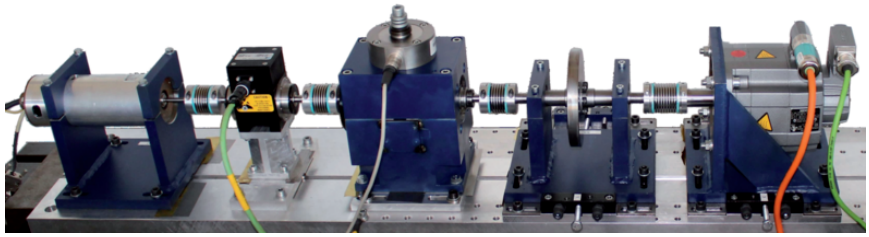

Fig. 10. Test bench used in the Paderborn University database

The acceleration of the bearing is captured using a piezoelectric accelerometer of model No. 336C04 PCB. The vibration signal is recorded in MATLAB files, with a sampling frequency of 64 kHz [32].

The selected operational condition, in conjunction with the geometric parameters, was utilized to ascertain the fault frequencies of the bearing components, as exemplified in Table 6.

Table 6. Parameters and frequencies of defects

Operating condition	Parameters	Frequencies
Rotational speed 900 rpm	Inner race diameter 24 mm	F_{ir} = 74.70 Hz
Load torque 0.7 Nm	Outer race diameter 31.1 mm	F_{or} = 45.29 Hz
Radial force 1000 N	Number of rolling element 8	F_c = 5.66 Hz
	Rolling element diameter 6.75 mm	F_{re} = 28.77 Hz
	Angle of contact 0°	

When the outer ring fails and the fault frequency is 45.29 Hz, the proposed approach (Fig. 1) is applied to the vibration signal.

3.2.1. Results

- Fig. 11 illustrates the noise removal from the vibration signal.
- Parameter (a) was optimized by selecting a value of 100, as this resulted in the highest correlation between the original signal and the observed sum of modes, as depicted in Table 7.
- The SVMD algorithm produces five modes through signal decomposition, which are illustrated in Fig. 12.

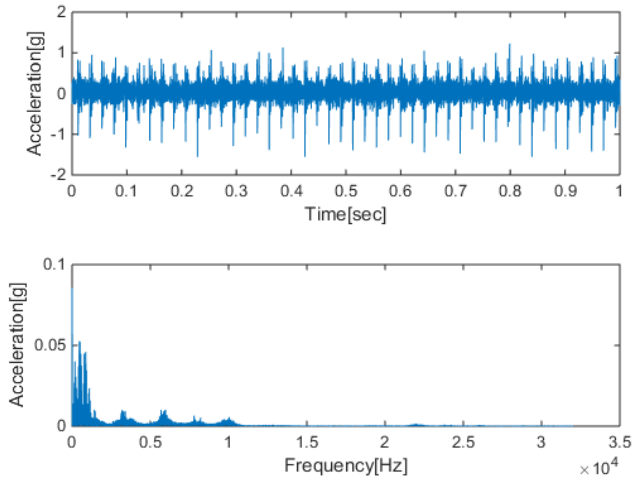

Fig. 11. Spectrum of vibration signal

Table 7. Correlation between signal and sum of modes

a	Correlation$\times 10^3$
100	2.9985
200	2.9849
300	2.9558
400	2.9760
500	2.9122

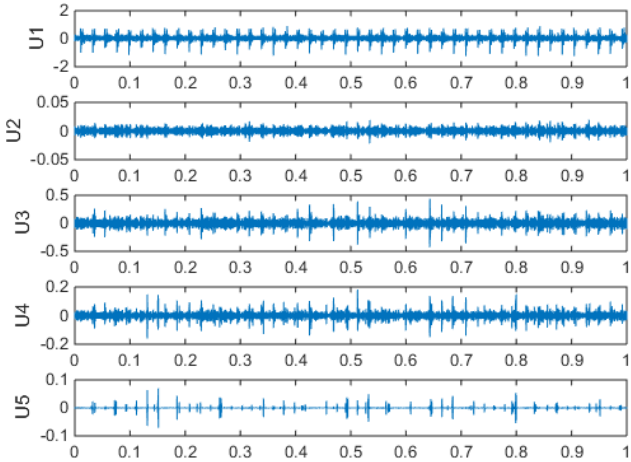

Fig. 12. The modes obtained after the decomposition

- Equations 20 and 21 are utilized to delineate the disordered and ordered components of the signal, respectively. These equations are based on the utilization of a predetermined threshold (denoted as 'S_{ie}') and the corresponding values of the weighted entropy index *WEI*, which are sourced from Table 8.

Table 8. *WEI* values of each mode

Modes	u_1	u_2	u_3	u_4	u_5
$10^4\times$WEI	4.2390	0.0033	0.6267	0.1311	0.0538

The threshold: $S_{ie} = Mean = 1.1933 \times 10^4$.

$$DP(t) = u_1(t)\,, \tag{20}$$

$$OP(t) = \sum_{k=2}^{5} u_k(t). \tag{21}$$

- The envelope spectrum (Figs. 13 and 14) displays a prominent peak with high amplitude at a frequency of 45.9 Hz for both the ordered and disordered parts, which is in close proximity to the fault frequency of the outer ring $F_{or} = 45.29$ Hz.

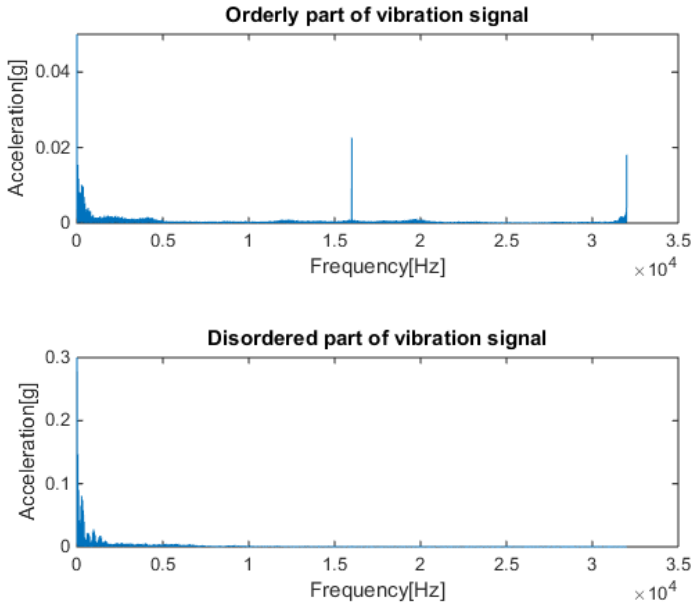

Fig. 13. Envelope spectrum of ordered and disordered parts

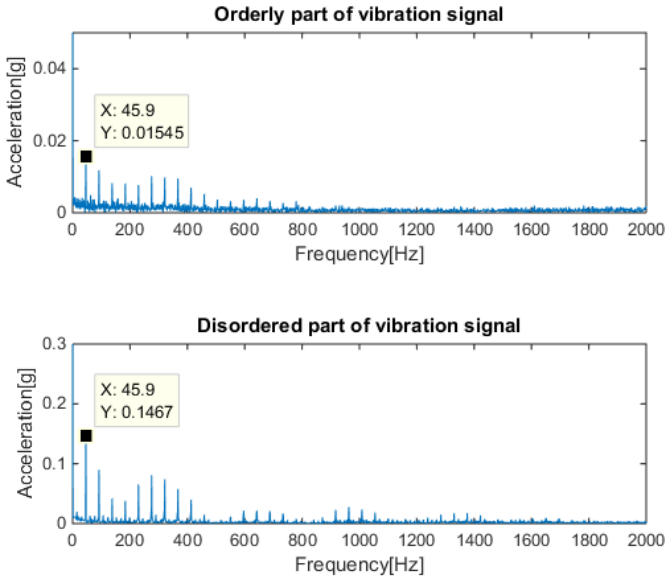

Fig. 14. Envelope spectrum zoom

3.3. Comparative evaluation of the results

Deconvolution, frequently used in the analysis of vibrational signals, involves an inverse operation of convolution [11]. The vibration signal can be interpreted as the result of convolution between the impulse component of the signal and the transfer function of the path between the fault source and the sensor [11]. There are different deconvolution methods, but we use the MCKD (Maximum Correlated Kurtosis Deconvolution) algorithm. The detailed steps of the MCKD algorithm are available in the reference [33].

In this subsection, we perform a comparison between the results obtained by the deconvolution methods and our proposed approach (Fig. 1).
The detection of defects using deconvolution methods involves two main steps [34]:

- Deconvolution of the vibration signal performed to extract the impulse component of the signal, which is related to the defect.
- Calculation of the envelope spectrum.

We apply the deconvolution method to a single vibration signal from the Paderborn University database, which was previously used in subsection 3.2.
The parameters of the MCKD algorithm are established as follows: number of iterations (N=10), filter size (T=100), period (P=450), order (M=1).

The envelope spectrum obtained after deconvolution (Fig. 15) shows a significant peak at a frequency of 52.73 Hz, which is close to the fault frequency of the outer ring at 45.29 Hz, but with an absolute error of 7.44 Hz. However, the proposed approach exhibits a peak at the frequency of 45.9 Hz.

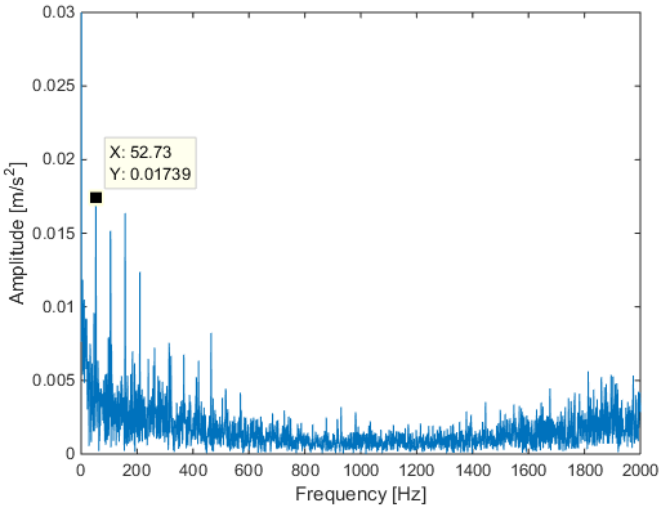

Fig. 15. Envelope spectrum obtained after the deconvolution

4. Conclusions

In this study, we analyze two vibration signals related to defects in the outer ring of bearings using a proposed approach that relies on the use of complementary methods. As a result of this approach, high-amplitude peaks are observed at the frequencies of defects. Detecting these defects from the spectra of the original vibration signals is challenging due to the presence of multiple peaks with a complex distribution in the spectrum. Due to the complexity of the spectrum shape, it is necessary to apply other methods to simplify its structure. This is how we have developed an approach based on dividing the signal into two parts using the SVMD method and a proposed new indicator called the weighted entropy index (*WKI*).

By combining kurtosis, entropy, and the Hojorth complexity parameter, we are able to reconstruct the *WKI*, which is used to evaluate the complexity of the simple signals obtained after decomposing the original signal. Moreover, the SVMD decomposition method requires the optimization of input parameters to ensure an effective decomposition. In this regard, we have developed an optimization algorithm to determine the input parameters.

A proposed threshold, equal to the average *WKI* of the simple signals (u), is used to separate the modes (u) into ordered and disordered states. Then, the sum of this latter mode can be used to construct two parts of the signal: one ordered and the other disordered. Through the comparison of the frequencies of the peaks in the spectrum with the frequencies of the faults in the bearing, which are determined based on geometric parameters and rotational speed, it becomes possible to detect faulty components in the bearing. The presence of peaks at different frequencies compared to the frequencies of defects in the bearing components leads to an

incorrect diagnosis and localization of the fault, making it challenging to determine accurately and identify the location of the defect.

References

[1] A. Nabhan, N.M. Ghazaly, A. Samy, and M.O. Mousa. Bearing fault detection techniques – a review. *Turkish Journal of Engineering, Sciences and Technology*, 3(2):1–18, 2015.

[2] P.P. Kharche and S.V. Kshirsagar. Review of fault detection in rolling element bearing. *International Journal of Innovative Research in Advanced Engineering*, 1(5):169–174, 2014.

[3] Y. Du, S. Zhou, X. Jing, Y. Peng, H. Wu, and N. Kwok. Damage detection techniques for wind turbine blades: A review. *Mechanical Systems and Signal Processing*, 141:106445, 2020. doi: 10.1016/j.ymssp.2019.106445.

[4] Z. Hameed, Y.S. Hong, Y.M. Cho, S.H. Ahn, and C.K. Song. Condition monitoring and fault detection of wind turbines and related algorithms: A review. *Renewable and Sustainable Energy Reviews*, 13(1):1–39, 2009. doi: 10.1016/j.rser.2007.05.008.

[5] K. Bouaouiche, Y. Menasria, and D. Khalfa. Diagnosis of rotating machine defects by vibration analysis. *Acta IMEKO*, 12(1):1–6, 2023. doi: 10.21014/actaimeko.v12i1.1438.

[6] S. Riaz, H. Elahi, K. Javaid, and T. Shahzad. Vibration feature extraction and analysis for fault diagnosis of rotating machinery-a literature survey. *Asia Pacific Journal of Multidisciplinary Research*, 5(1):103–110, 2017.

[7] M. Avoci Ugwiri, M. Mpia, and A. Lay-Ekuakille. Vibrations for fault detection in electric machines. *IEEE Instrumentation & Measurement Magazine*, 23(1):66–72, 2020. doi: 10.1109/MIM.2020.8979527.

[8] T. Liu, S. Yan, and W. Zhang. Time–frequency analysis of nonstationary vibration signals for deployable structures by using the constant-Q nonstationary gabor transform. *Mechanical Systems and Signal Processing*, 75:228–244, 2016. doi: 10.1016/j.ymssp.2015.12.015.

[9] K. Dragomiretskiy and D. Zosso. Variational mode decomposition. *IEEE Transactions on Signal Processing*, 62(3):531–544, 2014. doi: 10.1109/TSP.2013.2288675.

[10] M. Nazari and S.M. Sakhaei. Successive variational mode decomposition. *Signal Processing*, 174:107610, 2020. doi: 10.1016/j.sigpro.2020.107610.

[11] Y. Miao, B. Zhang, J. Lin, M. Zhao, H. Liu, Z. Liu, and H. Li. A review on the application of blind deconvolution in machinery fault diagnosis. *Mechanical Systems and Signal Processing*, 163:108202, 2022. doi: 10.1016/j.ymssp.2021.108202.

[12] T. Barszcz and N. Sawalhi. Fault detection enhancement in rolling element bearings using the minimum entropy deconvolution. *Archives of Acoustics*, 37(2):131–141, 2012. doi: 10.2478/v10168-012-0019-2.

[13] T. Barszcz and A. Jabłoński. A novel method for the optimal band selection for vibration signal demodulation and comparison with the Kurtogram. *Mechanical Systems and Signal Processing*, 25(1):431–451, 2011. doi: 10.1016/j.ymssp.2010.05.018.

[14] A. Moshrefzadeh and A. Fasana. The Autogram: An effective approach for selecting the optimal demodulation band in rolling element bearings diagnosis. *Mechanical Systems and Signal Processing*, 105:294–318, 2018. doi: 10.1016/j.ymssp.2017.12.009.

[15] D. Neupane and J. Seok. Bearing fault detection and diagnosis using Case Western Reserve University dataset with deep learning approaches: A review. *IEEE Access*, 8:93155–93178, 2020. doi: 10.1109/ACCESS.2020.2990528.

[16] K. Bouaouiche, Y. Menasria, and D. Khalifa. Detection of defects in a bearing by analysis of vibration signals. *Diagnostyka*, 24(2):2023203, 2023. doi: 10.29354/diag/162230.

[17] G. Chen, W. Xie, and Y. Zhao. Wavelet-based denoising: A brief review. In *2013 Fourth International Conference on Intelligent Control and Information Processing (ICICIP)*, pages 570–574, Beijing, China, 2013. IEEE. doi: 10.1109/ICICIP.2013.6568140.

[18] M. Rhif, B.A. Abbes, I.R. Farah, B. Martínez, and Y.-F. Sang. Wavelet transform application for/in non-stationary time-series analysis: A review. *Applied Sciences*, 9(7):1345, 2019. doi: 10.3390/app9071345.

[19] A. Dibaj, R. Hassannejad, M.M. Ettefagh, and M.M. Ehghaghi. Incipient fault diagnosis of bearings based on parameter-optimized VMD and envelope spectrum weighted kurtosis index with a new sensitivity assessment threshold. *ISA Transactions*, 114:413–433, 2021. doi: 10.1016/j.isatra.2020.12.041.

[20] Y. Li, W. Sun, R. Jiang, and Y. Han. Signal-segments cross-coherence method for nonlinear structural damage detection using free-vibration signals. *Advances in Structural Engineering*, 23(6):1041–1054, 2020. doi: 10.1177/1369433219886962.

[21] J. Yang, C. Zhou, and X. Li. Research on fault feature extraction method based on parameter optimized variational mode decomposition and robust independent component analysis. *Coatings*, 12(3):419, 2022. doi: 10.3390/coatings12030419.

[22] R.M. Mehmood, R. Du, and H.J. Lee. Optimal feature selection and deep learning ensembles method for emotion recognition from human brain EEG sensors. *IEEE Access*, 5:14797–14806, 2017. doi: 10.1109/ACCESS.2017.2724555.

[23] S.-H. Oh, Y.-R. Lee, and H.-N. Kim. A novel EEG feature extraction method using Hjorth parameter. *International Journal of Electronics and Electrical Engineering*, 2(2):106–110, 2014. doi: 10.12720/ijeee.2.2.106-110.

[24] Z. Wang, J. Zhou, J. Wang, W. Du, J. Wang, X. Han, and G. He. A novel fault diagnosis method of gearbox based on maximum kurtosis spectral entropy deconvolution. *IEEE Access*, 7:29520–29532, 2019. doi: 10.1109/ACCESS.2019.2900503.

[25] B. Bono, J. Arnau, R. Alarcón, and M.J. Blanca. Bias, precision, and accuracy of skewness and kurtosis estimators for frequently used continuous distributions. *Symmetry*, 12(1):19, 2019. doi: 10.3390/sym12010019.

[26] S. Kim, D. An, and J.-H. Choi. Diagnostics 101: A tutorial for fault diagnostics of rolling element bearing using envelope analysis in MATLAB. *Applied Sciences*, 10(20):7302, 2020. doi: 10.3390/app10207302.

[27] X. Ye, Y. Hu, J. Shen, R. Feng, and G. Zhai. An improved empirical mode decomposition based on adaptive weighted rational quartic spline for rolling bearing fault diagnosis. *IEEE Access*, 8:123813–123827, 2020. doi: 10.1109/ACCESS.2020.3006030.

[28] V. Kannan, H. Li, and D.V. Dao. Demodulation band optimization in envelope analysis for fault diagnosis of rolling element bearings using a real-coded genetic algorithm. *IEEE Access*, 7:168828–168838, 2019. doi: 10.1109/ACCESS.2019.2954704.

[29] P.H. Jain and S.P. Bhosle. Analysis of vibration signals caused by ball bearing defects using time-domain statistical indicators. *International Journal of Advanced Technology and Engineering Exploration*, 9(90):700, 2022. doi: 10.19101/IJATEE.2021.875416.

[30] C.R. Soto-Ocampo, J.M. Mera, J.D. Cano-Moreno, and J.L. Garcia-Bernardo. Low-cost, high-frequency, data acquisition system for condition monitoring of rotating machinery through vibration analysis-case study. *Sensors*, 20(12):3493, 2020. doi: 10.3390/s20123493.

[31] XJTU-SY bearing database. https://biaowang.tech/xjtu-sy-bearing-datasets/.

[32] Paderborn University database. http://mb.uni-paderborn.de/kat/datacenter.

[33] G.L. McDonald, Q. Zhao, and M.J. Zuo. Maximum correlated Kurtosis deconvolution and application on gear tooth chip fault detection. *Mechanical Systems and Signal Processing*, 33:237–255, 2012. doi: 10.1016/j.ymssp.2012.06.010.

[34] H. Cui, Y. Guan, and H. Chen. Rolling element fault diagnosis based on VMD and sensitivity MCKD. *IEEE Access*, 9:120297–120308, 2021. doi: 10.1109/ACCESS.2021.3108972.